PNAS RESEARCH ARTICLE | NEUROSCIENCE

Comparative connectomics reveals noncanonical wiring for color vision in human foveal retina

Yeon Jin Kim[a], Orin Packer[a], Andreas Pollreisz[b], Paul R. Martin[c], Ulrike Grünert[c], and Dennis M. Dacey[a,d,1]

Edited by Martin Banks, University of California, Berkeley, CA; received January 11, 2023; accepted March 31, 2023

The Old World macaque monkey and New World common marmoset provide fundamental models for human visual processing, yet the human ancestral lineage diverged from these monkey lineages over 25 Mya. We therefore asked whether fine-scale synaptic wiring in the nervous system is preserved across these three primate families, despite long periods of independent evolution. We applied connectomic electron microscopy to the specialized foveal retina where circuits for highest acuity and color vision reside. Synaptic motifs arising from the cone photoreceptor type sensitive to short (S) wavelengths and associated with "blue–yellow" (S-ON and S-OFF) color-coding circuitry were reconstructed. We found that distinctive circuitry arises from S cones for each of the three species. The S cones contacted neighboring L and M (long- and middle-wavelength sensitive) cones in humans, but such contacts were rare or absent in macaques and marmosets. We discovered a major S-OFF pathway in the human retina and established its absence in marmosets. Further, the S-ON and S-OFF chromatic pathways make excitatory-type synaptic contacts with L and M cone types in humans, but not in macaques or marmosets. Our results predict that early-stage chromatic signals are distinct in the human retina and imply that solving the human connectome at the nanoscale level of synaptic wiring will be critical for fully understanding the neural basis of human color vision.

marmoset and macaque retina | neural circuitry | human vision | color vision | comparative connectomics

Significance

Comparative connectomics—the study of neural circuits at synaptic resolution across species or the life span—promises to reveal how evolution modifies the nervous system to shape behavior and perception. Here, we compare the synaptic connectome for a color-coding circuit in the human retina with the comparable circuits in both marmoset and macaque monkeys. We discover a circuit in humans that is absent in marmosets and show further that for the human retina synaptic motifs do not follow the canonical architecture established in macaque monkeys. Our results may help to explain why some aspects of human color perception are not well predicted from physiological studies of macaque monkey visual system.

Model organisms such as macaque monkey provide a broad scaffold for understanding vertebrate neural systems (1, 2), yet nerve circuits must be altered in some way by evolution to modify perception and behavior across species (3, 4). Thus, understanding how synaptic wiring differs across closely related species can help to explain the underlying logic of neural circuit design (5–8). This undertaking is especially critical for the human brain, where only limited homology can be made with monkey brain organization (9, 10)—a fact which may not be surprising given over 25 My of independent evolution in these two distinct primate lineages (11).

Humans and many nonhuman primates are trichromatic: The image projected onto the retina is initially sampled by three cone photoreceptor types with peak sensitivities at short (S), middle (M), or long (L) wavelengths (12). But, the cones are not labeled lines for color: Their photon catch rates are determined by both wavelength and photon number (flux) (13), meaning information about wavelength must be extracted by comparing signals across cone types. This task is accomplished in postreceptoral neural circuits by antagonistic or opposing interactions between cone signals (14). An enduring question about such opponent circuitry is the mismatch between fundamental cone-opponent mechanisms established physiologically in macaques (15) vs. the color-opponent channels of human color perception (16–21). Specifically, the perceptual color opponent axes posited to link the unique hues, red, green, blue, and yellow with underlying mechanisms (16, 17) do not align with the cone opponent axes (S vs. L+M (hereinafter or LM) and L vs. M) identified physiologically at the level of the retina and lateral geniculate nucleus (15). It has been suggested that higher-order mechanisms amplify and combine the cardinal S vs. LM with the L vs. M opponent signals (22–24).

In the best-understood model for human color coding, the macaque monkey, S cones give rise to two parallel signaling pathways specialized for color processing (25). First, each S cone is selectively contacted by a morphologically distinct ON-type bipolar cell (26, 27), creating a circuit that responds to light increment (S-ON pathway). For consistency with previous studies (28, 29), we refer to the S-ON-type bipolar cell as "blue cone bipolar" (BB), but it should be noted that any color percepts arising from the output of this bipolar type remain unknown.

Each S cone in macaque fovea is also selectively contacted by a single "flat midget" bipolar (FMB) cell (30, 31), forming a circuit that responds to light decrements (S-OFF pathway). The BB (S-ON) and FMB (S-OFF) bipolar cells, respectively, contact S-ON and S-OFF ganglion cell types (32, 33), creating parallel color-coding output pathways.

Author contributions: Y.J.K. and D.M.D. designed research; Y.J.K. and D.M.D. performed research; Y.J.K., O.P., A.P., U.G., and D.M.D. contributed new reagents/analytic tools; Y.J.K., P.R.M., and D.M.D. analyzed data; and Y.J.K., P.R.M., U.G., and D.M.D. wrote the paper.

The authors declare no competing interest.

This article is a PNAS Direct Submission.

[1]To whom correspondence may be addressed. Email: dmd@uw.edu.

This article contains supporting information online at https://www.pnas.org/lookup/suppl/doi:10.1073/pnas.2300545120/-/DCSupplemental.

Published April 25, 2023.

In both pathways, the S cone signals are opposed by signals drawn from both L and M cones to generate either blue-ON/yellow-OFF or blue-OFF/yellow-ON cone opponent ganglion cell receptive fields. A hallmark of these pathways in macaque is the purity of the excitatory S cone signal: S-ON and S-OFF bipolar cells draw input selectively only from S cones. Moreover, while L and M cones are coupled by gap junctions at the synaptic pedicle, S cones remain electrically isolated from their L and M cone neighbors (34). These S cone pathways in macaque have been characterized by detailed electron microscopic circuit reconstruction in multiple studies (26, 30, 31, 33, 35) (*SI Appendix*, Fig. S10) and are viewed as defining an S vs. LM cardinal axis of cone-opponent processing applicable to human color vision (36).

By contrast with macaque monkey, detailed characterization of human retinal circuitry is limited (27, 29, 37), and a single previous study suggested the absence of the S-OFF flat midget circuit at presumed S cones (38). Similarly, a light microscopic immunolabeling study (39) suggested that the S-OFF pathway is absent in marmosets, despite the presence of an S-ON ganglion cell circuit homologous to that identified in macaques (40, 41). The incidence of color vision defects due to changes in cone photopigment spectral tuning is substantially lower in macaques than that in humans and marmosets (42–44), but whether there is parallel interspecies variability in the color circuitry postsynaptic to the cones is unclear. Further, in nonprimate mammals, the circuitry linked to S cones appears highly variable (45) suggesting that evolutionary demands may act principally at the nanoscale of microcircuitry. Molecular profiling studies show that cell types in macaque retina can be mapped onto counterparts in humans (46, 47); yet, such studies do not address the question of how synaptic connectivity may be modified across closely related species (48). Thus, our goal here was to apply connectomic reconstruction methods to directly determine the nature of the S cone circuits in both human and marmoset foveal retina, applying identical methods to those previously used to analyze macaque monkey fovea (26, 30, 31, 49). We discover the presence of a distinctive S-OFF pathway in the human retina while also demonstrating its absence in marmosets. Moreover, in humans, both S-ON and S-OFF circuits deviate from the canonical wiring scheme to draw input from L and M cones. Because small differences in retinal wiring can shift the spectral tuning of color opponent cells (31), these anatomical results predict that early-stage chromatic signals in primate visual system will show species specificity. The results further imply that macaque retinal circuitry does not provide a full accounting for the initial stages of human color vision.

Results

Identification of S Cones in the Human and Marmoset Central Retina. Marmoset, human, and a previously studied macaque (31) retinal volume were derived from a comparable central retinal location within 1 to 2 degrees of the foveal center. The imaged volumes extended from the layer of pedicles and their axons (*SI Appendix*, Fig. S1 *A* and *B*, *Top*, Henle fiber layer or HFL) to the ganglion cell layer (*SI Appendix*, Fig. S1 *A* and *B*, *Bottom*, ganglion cell layer or GCL). Previous immunohistochemical studies in humans (50), macaques (51), marmosets (52), and other primate species (53) have established the relative sparseness of the S cone population (<10%) at the fovea. It is also known that in the central retina of marmosets (39, 54) and macaques (30, 31), S cone pedicles are smaller than LM cone pedicles. Thus, we first surveyed all cones in our marmoset volume and tentatively identified the S cone pedicles by size alone (Fig.1*A* and *SI Appendix*, Fig. S1*D*). We then reconstructed the neurons postsynaptic to these putative S cones. A clear population of likely S cone pedicles was not conspicuous in the human retina (Fig. 2*A* and *SI Appendix*, Fig. S1*C*), and previous electron microscopic evidence suggested that they may be variable in size and morphology (38, 55). In our human volume, we thus made full-circuit reconstructions to identify S cones.

In macaque monkey retina, the major S-ON pathway originates with the blue cone bipolar cell (BB) (28, 56–58). Typically, the dendritic terminals from one to two BB cells converge on an S cone and occupy the invaginating central positions at every ribbon synapse (26, 31). The BB cell is in turn presynaptic to a distinctive ganglion cell type, referred to as the small bistratified cell (31, 33). By contrast, for the LM cones, the primary ON pathway arises from an invaginating midget bipolar type (IMB) and its postsynaptic partner, the midget ganglion cell; near the fovea, this pathway creates a one-to-one ("private-line") connection from cone to midget bipolar to midget ganglion cell (49). Both the BB and IMB pathways have been identified in marmoset and human retina (27, 40, 59–65). These features allowed us to identify (66) each S cone in both our marmoset and human retinal volumes. The identities based on these morphological criteria are supported by principal component analysis and unsupervised classification using measured parameters from the human and macaque and marmoset volumes (*SI Appendix*, Fig. S3 *C–E*).

Morphology of the Marmoset S-ON Circuit. Marmoset S cone pedicles can be distinguished from those of neighboring LM cones not only by their relatively small size [Fig. 1*A*; LM pedicle diam (μm), 9.4 ± 0.7, n = 10; S pedicle diam (μm), 6.1 ± 0.4, n = 9; see also figure 8 in Lee and Grünert, 2007 (54)], but also by the presence of fewer synaptic ribbons [Fig. 1*B*; LM cones: mean ± SD = 23.76 ± 1.71, n = 45; S cones: mean ± SD = 12.33 ± 1.00, n = 9; see also Puller et. al., 2007 (67)] and the absence of telodendria and pedicle-to-pedicle contact [presumed gap junction loci (34, 68)] with surrounding LM cones. By contrast, the LM pedicles each give rise to one or two fine diameter telodendria (Fig. 1*A*, arrows, *SI Appendix*, Fig. S2 *A–D*) that contact either the pedicle body or the telodendritic tips of neighboring cones (LM cone–cone contact: mean ± SD = 2.44 ± 0.97, n = 45). A cluster of six completely reconstructed cone pedicles from the marmoset volume (Fig. 1*A*) illustrates these distinguishing morphological features of the S cone pedicle. We could identify 9 out of 145 cones in marmosets as S cones (~6%) by their morphology and connectivity. The irregular, patchy distribution (*SI Appendix*, Fig. S3*B*) and the percentage of S cones are a close match to previous immunolabeling studies (52).

We reconstructed all bipolar cells that formed invaginating central elements at the synaptic triads of all 13 presynaptic ribbons for one S cone (Fig. 1*B*, blue processes, red arrowheads). Three invaginating bipolar cells selectively target this S cone and give rise to all the central elements for this pedicle (Fig. 1 *C* and *D*); additional dendrites either extend to contact other S cone pedicles or end blindly in the outer plexiform layer (OPL). Each of the three bipolar cells has an axon terminal that terminates near the inner border of the inner plexiform layer (IPL; S5) (Fig. 1 *C* and *E*) following previous descriptions of DiI-labeled and immunolabeled BBs in both macaque (28, 30, 33, 57) and marmoset (69, 70) retina. The axon terminals enwrap and make multiple synaptic contacts with the inner dendritic tree of a morphologically distinct ganglion cell with dendrites that stratify near the inner border of the IPL (S4-5) and also extend branches to the outer border of the IPL (S1-2). The ganglion cell corresponds in dendritic morphology to the small bistratified ganglion cell (SBGC) type previously described in both marmoset and macaque retina (25, 27, 41, 59, 71, 72). Taken together, these features confirm the pedicle's identity as an S cone

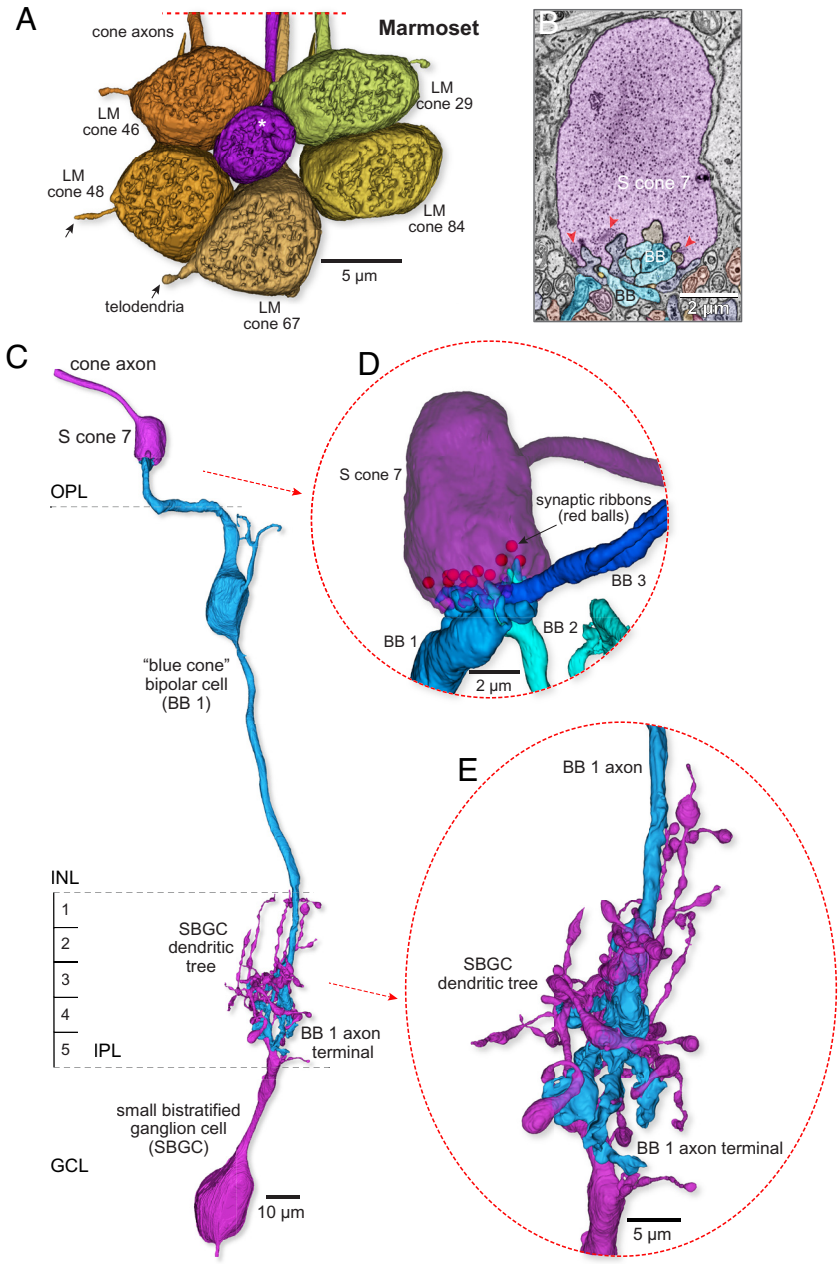

Fig. 1. Identification of the S-cone pathway in marmoset retina. (*A*) Volume reconstructions of a cluster of 6 cone pedicles in parafoveal retina (~300 µm eccentricity). The view is toward the outer retina directed at the pedicle synaptic face. One of the 6 pedicles shown (S cone 7, purple, white asterisk, at center of the pedicle cluster) is notably smaller in diameter than the surrounding cones (LM cones, yellow to brown). The LM cone pedicles in the cluster were interconnected by a few, fine-diameter telodendria (arrows; see also *SI Appendix*, Fig. S2 *A–D*). (*B*) Single-layer SEM image shows a section through the S cone pedicle marked with the white asterisk in *A*. All central elements (located opposite to synaptic ribbons, red arrowheads) arose from a morphologically distinct BB cell; flat and invaginating midget bipolar connections were lacking. (*C*) Complete reconstruction of a single Blue cone bipolar (BB) circuit. The BB cell (medium blue) densely contacts the S cone and projects an axon to the inner border of the IPL where it makes predominant synaptic output to a small bistratified ganglion cell type (SBGC, purple). (*D*) Rotated and zoomed inset shows that S cone 7 was targeted by two additional BB cells (BB 2 and BB 3). BBs 1 to 3 accounted for all central elements at the S cone pedicle (synaptic ribbon positions indicated by the red balls). (*E*) Rotated and zoomed view of the BB 1 to SBGC projection shows the intimate enwrapping of the BB 1 cell axon terminal with the SBGC inner dendrites.

and the bipolar identity as BB cells conveying S-ON signals to the inner retina.

Convergent S and LM Cone Connectivity of the Human S-ON Circuit. The first unusual feature of the human cone pedicles in our volume is that *all* pedicles were connected by telodendritic processes (Fig. 2*A* and *SI Appendix*, Fig. S2 *E–I*). Similar observations were made in previous studies of human retina (38, 55, 73), implying that in humans unlike in nonhuman primates, the S cones form electrical junctions with LM cones. To unequivocally identify the human S cones, we therefore had to first show each was presynaptic to BB cell–SBGC circuitry. Examples of the BB circuit motif, and comparison with connections of LM cones, are shown in Figs. 2 and 3. Once a human S cone pedicle had been identified by its BB connection (Fig. 2 *A–C*), it could also be distinguished from neighboring LM cones by synaptic ribbon numbers (Fig. 2*B*, LM cones: mean ± SD = 25.76 ± 3.14, n = 45; S cones: mean ± SD = 17.71 ± 2.64, n = 17). Moreover, all S cones are linked to their LM cone neighbors by telodendritic contacts (Figs. 2*A* and 7 and *SI Appendix*, Fig. S2 *E–I*) via the pedicle body (*SI Appendix*, Fig. S2*F*) and/or the telodendritic tips (*SI Appendix*, Fig. S2 *G* and *H*) of neighboring cones (S–LM cone–cone contact: mean ± SD = 4.12

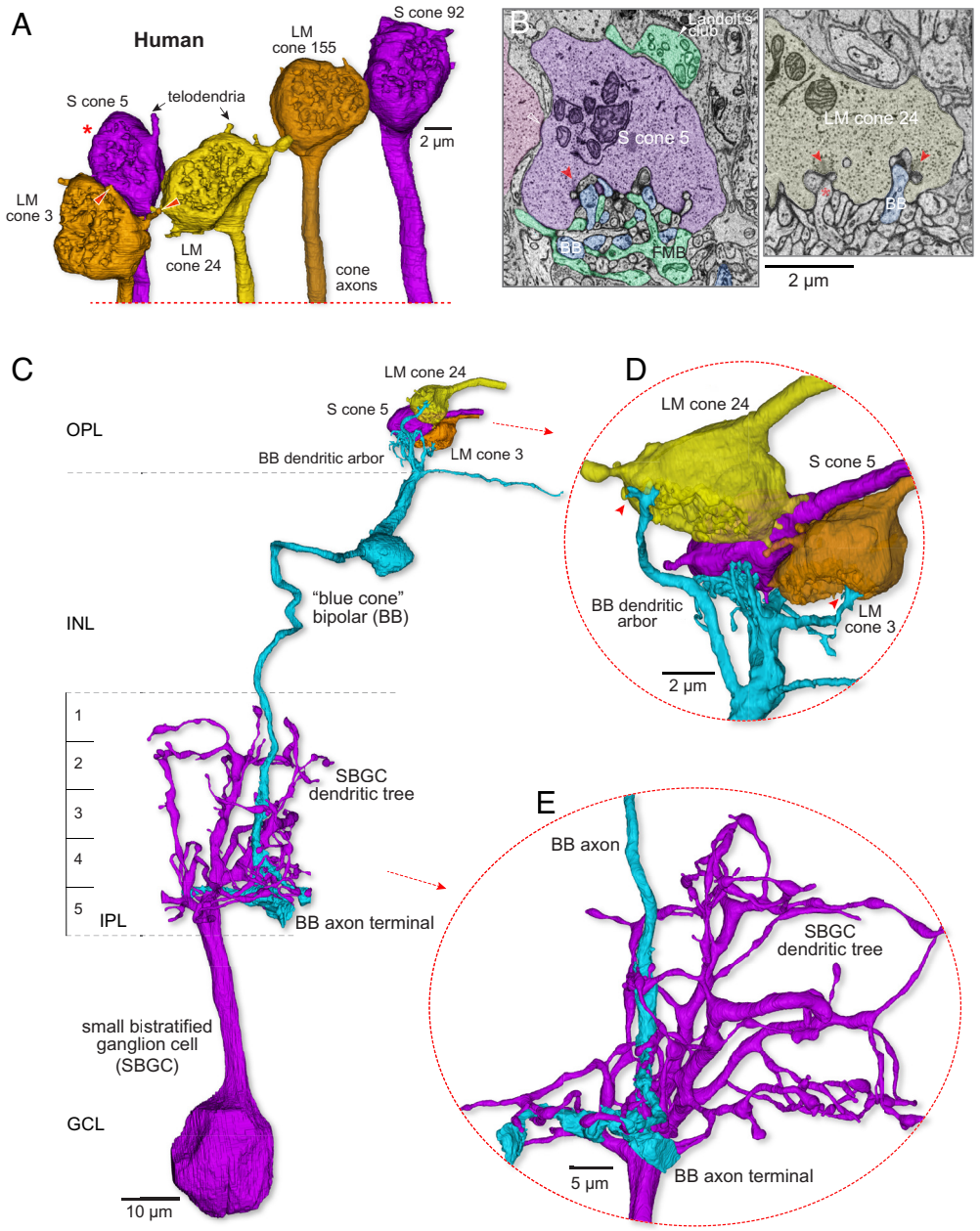

Fig. 2. Identification of the S-cone, blue cone bipolar synaptic pathway in human retina with mixed cone-type connectivity. (*A*) Volume reconstructions of a cluster of 5 cone pedicles in parafoveal retina (~500 µm retinal eccentricity). The view is toward the outer retina directed at the pedicle synaptic face. Two of the 5 pedicles shown were identified as S cones (S cones 5 and 92, purple) by their postsynaptic connectivity. All cone pedicles (LM cones, yellow to brown), including the S cones, were linked to their neighbors by distinctive telodendritic contacts (arrows, red arrowheads) extending from the pedicle base. The cone axons extend vertically downward beyond this image. (*B*, *Left*) a section through the S cone marked with the red asterisk in *A* illustrates a blue cone bipolar (BB) dendrite terminating as a central element (red arrowhead points to synaptic ribbon). The flat midget bipolar (FMB, teal) is also shown along with part of its Landolt's club (white arrowhead). A putative site of S–LM cone gap junction is indicated by the open white arrowhead. The complete reconstruction of this blue cone bipolar cell is shown in (*C*–*E*). (*B*, *Right*) example of the same BB cell (blue) as in the *Left* panel forming an invaginating central element at a synaptic triad (arrowhead) of LM cone 24; a comparable central element arising from an invaginating midget bipolar (asterisk) is also indicated. (*C*) The BB cell (light blue) densely contacts the S cone and projects an axon to the inner border of the IPL where it makes predominant synaptic output to a small bistratified ganglion cell type (SBGC, purple). (*D*) A rotated and zoomed view of panel (*C*) (*Top*) shows that this BB (BB 1) cell not only makes dense contact with S cone pedicle 5 but also makes sparse invaginating contacts (red arrowheads) with neighboring LM cone pedicles 24 and 3. (*E*) A rotated and zoomed view of the BB to SBGC projection shows the intimate enwrapping of the BB cell axon terminal with the SBGC inner dendrites.

± 1.36, n = 17; LM–LM cone–cone contact: mean ± SD = 8.11 ± 1.85, n = 45). Using this approach, we identified 16 out of 195 cones in human as S cones (~8%) in our volume (*SI Appendix*, Fig. S3*A*).

A second distinctive feature of the human S cone circuitry was the promiscuous connectivity of the BB cell. The canonical BB cell in both macaques and marmosets shows cone type selectivity: Dendrites bypass LM cones to seek and collect input from multiple widely spaced S cones. Selective targeting of S cones is also found in mouse (74), ground squirrel (75), and rabbit (76) retina, suggesting that this synaptic motif reflects the ancestral mammalian pattern. In the human retina, the BB cell also densely contacts S cones and can project dendrites long distances to target multiple S cones. But in contrast to marmoset and macaque BB cells, the human BB cell is also consistently postsynaptic to the LM cones which neighbor the primary S-cone target (Fig. 2 *B*, *Right*, Figs. 2 *C* and *D* and 7*C*; percent synaptic input: from S cone, mean ±

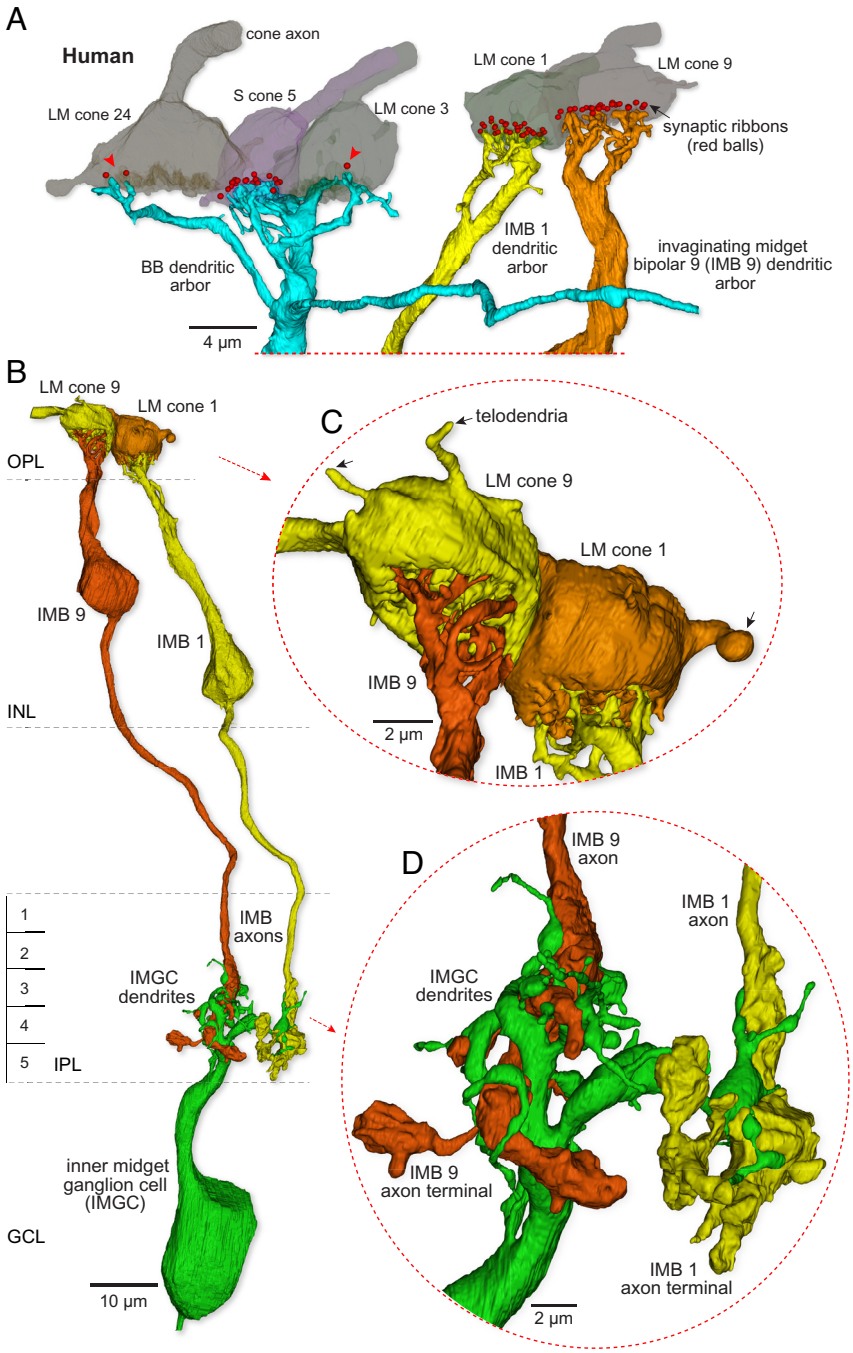

Fig. 3. The LM cone, inner-ON midget pathway in human retina is distinct from the blue cone bipolar pathway. (*A*) At *Left* is another view of the BB bipolar dendritic arbor shown in Fig. 2 (*C* and *D*). The pedicles of LM cones 24 and 3 and S cone 5 are shown in partial transparency and red balls show presynaptic ribbons targeting this BB cell. The BB cell makes dense contacts with the S cone pedicle (18 synaptic contacts as central elements) and sparse contact with the neighboring LM cones (3 central elements indicated by the red arrowheads). At *Right*, two additional LM cone pedicles (LM cones 1 and 9) and the dendritic arbors of two IMB cells (IMB 1 and 9) forming private-line connections with these pedicles are shown. (*B*) Complete reconstruction of the inner-ON midget circuit for each of the two LM cones shown on the *Right* in (*A*) (view is rotated). Each of the IMBs (IMBs 1 and 9) forms an axonal arbor that provides most of its synaptic output to a single inner midget ganglion cell (IMGC). (*C*) Zoomed and rotated views showing dendritic invaginations into the synaptic face of each pedicle and the single-cone connections of the IMB cells. (*D*) Zoomed view of the links between the two IMB axon terminals (yellow and orange) and the small dendritic tree of the IMGC.

SD = 87.92 ± 9.04; from LM cone, mean ± SD = 12.08 ± 9.04, n = 14). The BB contacts appear as central elements at the LM cone synaptic ribbon (Fig. 2 *B*, *Right*). By contrast to the BB cells, the human IMB cells tend to restrict dendritic terminals to single LM cones (Fig. 3 *A* and *C*; percent synaptic input: from LM cone, mean ± SD = 97.98 ± 6.70; from neighboring LM cone, mean ± SD = 2.02 ± 6.70, n = 11; 10 of 11 reconstructed IMB cells were completely private).

The axonal projection of human BB cells terminates near the inner border of the IPL and as expected synapses densely with the SBGC type (27) (Fig. 2 *C* and *E*; percent synaptic input: mean ± SD = 80.16 ± 9.53, n = 3). By contrast, the human IMB cells form small, globular axon terminals that extend vertically through most of the inner half of the IPL (Fig. 3 *B* and *D*) (S3-5) where they contact inner-ON midget ganglion cells. Inner-ON midget ganglion cells form a small cluster of terminal dendrites that enwrap

and receive almost all ribbon synaptic input from ON midget bipolar cells (Fig. 3 *B* and *D*).

The Private-Line Midget Circuit Is Absent at Marmoset S Cones. Light microscopic immunolabeling suggested that marmoset S cones lacked an output to an FMB type (39), which was surprising given the clear identification of this pathway in the macaque monkey (30, 31). We thus sought to substantiate or refute the previous light microscopic result at the EM level. As shown in Fig. 1, relative to the S cone pedicles, marmoset LM pedicles are much larger, contain nearly twice as many synaptic ribbons, and give rise to 1 or 2 narrow telodendritic extensions that interconnect LM cones (Fig. 4 *A* and *B*). Both IMB and FMB types make extensive contact with a single LM pedicle to initiate private-line pathways (Fig. 4*B*). Both midget bipolar types show one thick primary dendrite that extends to the base of the pedicle before dividing into many fine terminal branches. The FMB terminals tend to encircle the IMB terminals and contact the pedicle base near the synaptic triad. The axonal arbors of the IMB and FMB cells terminate broadly across the inner and outer ~40% of the IPL (Fig. 4*B*; S1-2; S4-5), respectively. Each bipolar terminal arbor forms a large globular mass with little branching. Inner-ON and outer-OFF midget ganglion cells form small finely branched dendritic arbors that enwrap the IMB and FMB axon terminals, respectively (Fig. 4 *C* and *D*). Both midget bipolar types rarely made synaptic output to other ganglion cells, and midget ganglion cells received most of their bipolar input from their primary midget bipolar partners, completing the intraretinal private-line pathway.

To determine whether such a flat midget bipolar (or other S-selective OFF bipolar type) was present in marmosets, we reconstructed all processes contacting a single S cone pedicle (S cone 7; Fig. 5*A*) to their cells of origin. We found a large number of

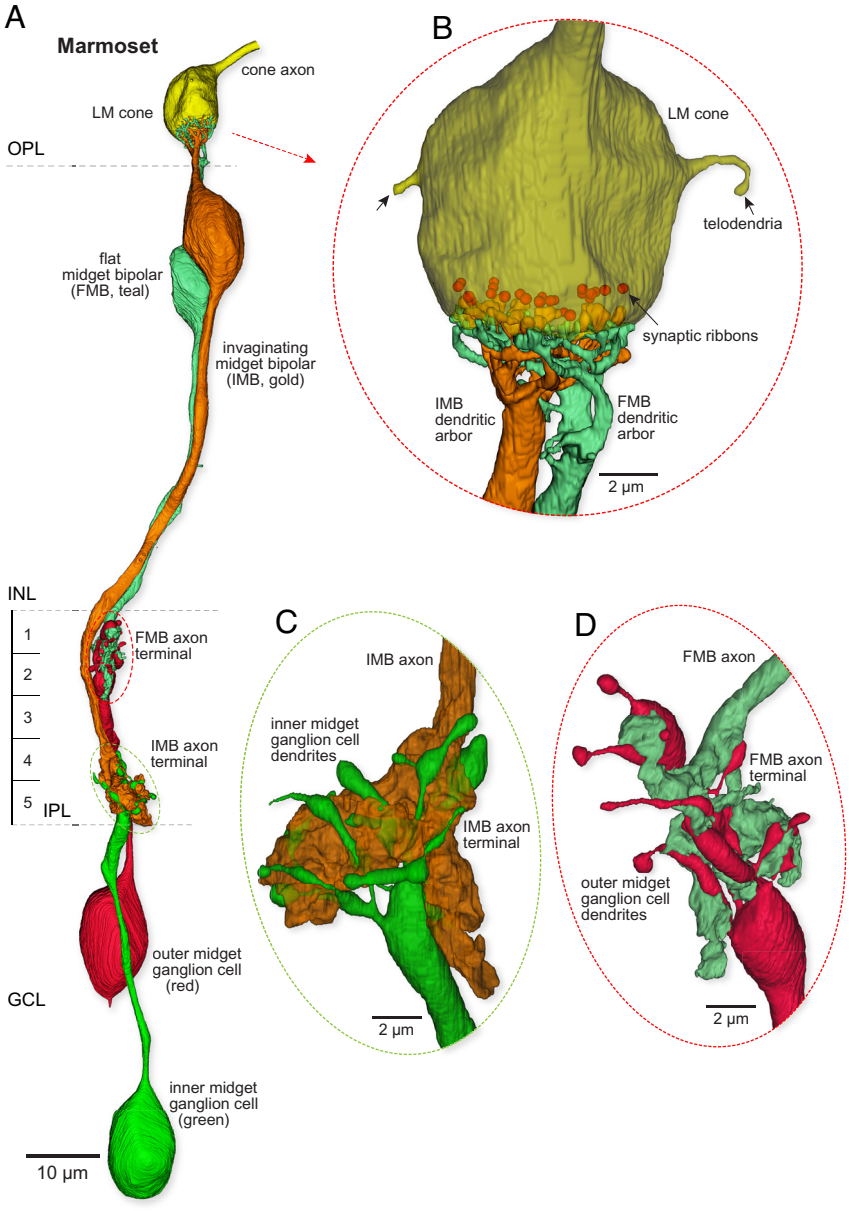

Fig. 4. Reconstruction of the private-line midget circuit in the marmoset: LM cones possess both outer-OFF and inner-ON circuits. (*A*) An LM cone pedicle (yellow at top) is selectively presynaptic to a single invaginating midget bipolar (IMB; gold) and a single flat midget bipolar (FMB; teal) cell. These bipolar cells connect to single inner-ON (green) and outer-OFF (red) midget ganglion cells. (*B*) Zoomed and rotated views of the IMB and FMB dendritic terminations at the cone pedicle synaptic face (ribbons are indicated as red balls, scaled to approximately match actual ribbon size). The IMB dendrites form central elements in the synaptic triad, whereas the FMB dendrites make flat contacts with the pedicle base. Note marmoset LM cones give rise to only few and very fine telodendria, indicated by the arrows. (*C* and *D*) Zoomed and rotated views of the contact from the IMB to an inner midget ganglion cell (*C*) and from the FMB to an outer midget ganglion cell (*D*).

flat contacts at the pedicle surface, but they arose from either BB cells (Fig. 1), H1 and H2 horizontal cells (Fig. 5 *B*–*E*), or from multiple nonmidget, i.e., diffuse bipolar (DB) cell types (Fig. 5*A* and *SI Appendix*, Figs. S4–S7). By completely reconstructing the DB cells, we were able to identify seven cells and sort them into three inner-stratifying, presumed ON-bipolar types (5 cells) and one outer stratifying, presumed OFF bipolar type (2 cells) (Fig. 5*A* and *SI Appendix*, Figs. S4–S7). To date, four OFF DB types (DB1, DB2, DB3a, and DB3b) and four ON types (DB4, DB5, DB6, and Giant bipolar) are recognized (28, 77). Within our small sample, we did not attempt to type every reconstructed DB cell and here distinguish them as DB 2/3 (OFF type) and DB4/5 (ON types) along with a Giant bipolar (GB). Each of the seven DB cells made only very sparse contacts with the pedicle (mean of 2.4 flat synaptic contacts/DB cell) (*SI Appendix*, Figs. S4–S7). We reconstructed all bipolar cells in contact with two additional S cones and also identified bipolar cell contacts with the other 5 complete S cones in our volume and never observed midget bipolar contacts to any S cone. In sum, our volume reconstructions confirm and extend previous evidence that marmoset retina lacks an S cone connecting FMB circuit. Moreover, we found that the great majority of synaptic contacts with bipolar cells were directed to ON-bipolar pathways (either BBs or inner-DBs 4/5) (54).

Identification of a Noncanonical Human S-OFF Midget Circuit. In macaque central retina, multiple EM reconstruction studies (30, 31, 35) (*SI Appendix*, Fig. S10) found that each S cone pedicle made a strict private line connection with an individual FMB (hereinafter S-FMB). These S-FMBs in turn established a private-line output to a single, presumed S-OFF midget ganglion cell. Here, we show that in human retina, an FMB cell is clearly present at each S cone, but that these S-FMBs lack the canonical private

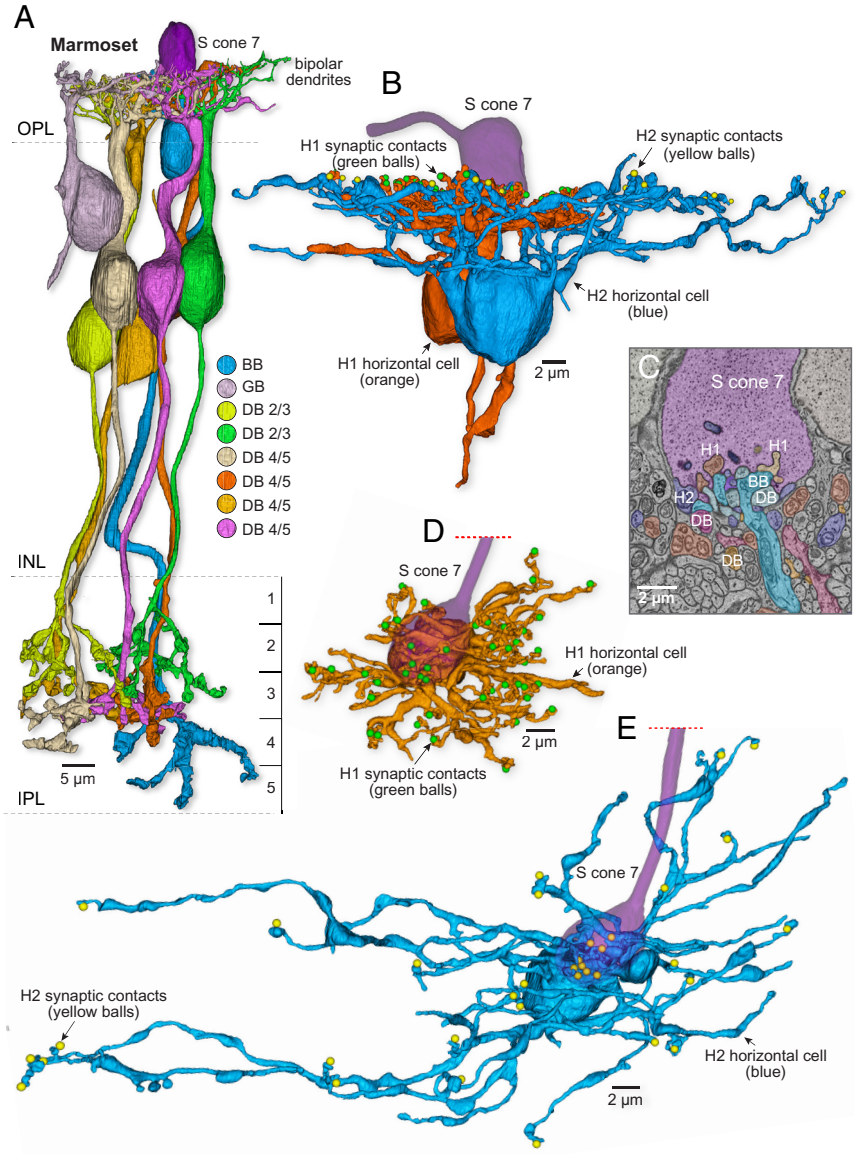

Fig. 5. Marmoset S cones lack an OFF-midget circuit. (*A*) S cone 7 sparsely contacted seven diffuse bipolar (DB) cells in addition to the three BB cells shown in Fig. 1; each DB cell is shown in a different color (further details about the DB types shown are given in *SI Appendix*, Figs. S4–S7). (*B*) S cone 7 was also contacted by both H1 (5 cells) and H2 (1 cell) horizontal cell types; one of the H1 cells and the H2 cell are shown in vertical view (green and yellow balls represent cone ribbon synapses contacted by either an H1 or H2 lateral element, respectively). (*C*) Single-layer SEM image through S cone pedicle 7 shows the processes of cells contacting this S cone, including H1 and H2 horizontal cells, blue-cone (BB) bipolar cells, and a diversity of diffuse (DB) bipolar types. No flat midget bipolars were seen at this or other S cones in this volume. (*D* and *E*) Examples of the same H1 cell (orange) and H2 cell (blue) shown in (*B*) that made numerous contacts with this S cone in horizontal view (direction from outer to inner retina). H2 cells (9 lateral element contacts with S cone 7; blue balls) are larger and more sparsely branching than the compact H1 cells (7 lateral element contacts; green balls).

line configuration, combining input from both LM and S cones (Fig. 6). First, similar to BB cells, human S-FMB cells extended multiple dendritic branches to make contacts with neighboring LM cones (Figs. 6 *A* and *B* and 7*C*; percent synaptic input; from LM cone, mean ± SD = 21.64 ± 4.13; from S cone, mean ± SD = 78.36 ± 4.13, n = 5). Second, the ganglion cells that were postsynaptic to the S-FMB cells also received a significant convergent synaptic input from a second LM cone-connected to an FMB cell (Figs. 6 *A* and *D* and 7*C*; percent synaptic input: from LM-FMB, mean ± SD = 15.38 ± 15.14; from S-FMB, mean ± SD = 82.44 ± 15.31, n = 4). Both of these synaptic motifs predict that this S-OFF midget pathway would show an excitatory receptive field center with contributions from S and some combination of L and M cones.

Human OFF Midget Bipolar Cells Possess a Landolt's Club. The Landolt's club is a conspicuous feature of certain bipolar cell types in bird, reptile, and amphibian retina (78–80), where they appear as large dendritic appendages that extend beyond the OPL to reach

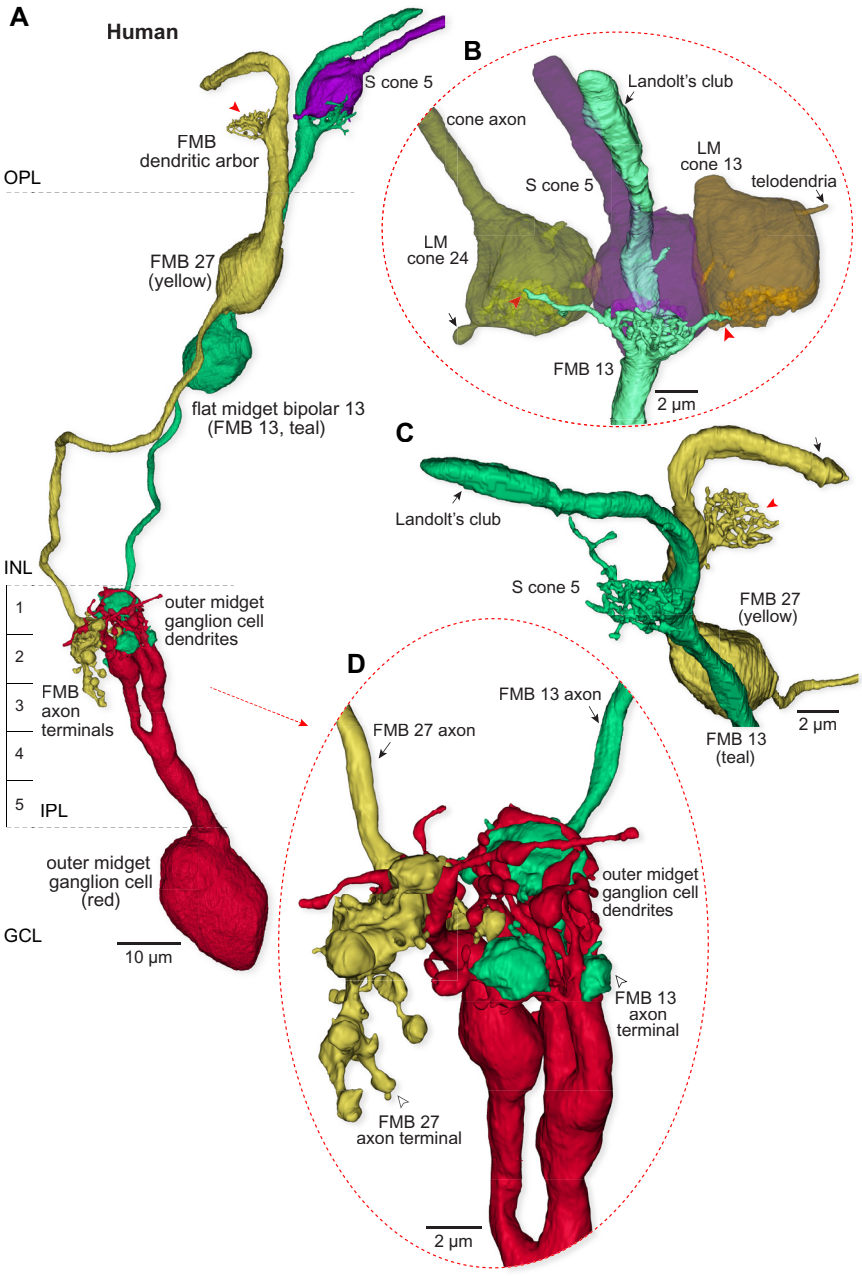

Fig. 6. Human S cones possess an OFF-midget circuit with combined S and LM input connectivity. (*A*) OFF midget circuit linked to the same S cone pedicle (S cone 5, purple) identified in Fig. 2 by its BB bipolar circuitry (purple). The FMB cell (teal, FMB13) dendrites densely carpet the synaptic face of the S cone pedicle and also send single branches to three neighboring LM cones (two are visible in *B*). The axon terminal of this S-FMB cell contacts a single outer-OFF midget ganglion cell (red) contributing 34 ribbon synaptic inputs. A second FMB cell (yellow, FMB 27) with a private-line connection to a neighboring LM cone (position indicated by red arrowhead) also projects to this ganglion cell contributing an additional 16 ribbon synaptic inputs. (*B*) Zoomed and rotated views of the FMB dendritic termination (teal) at the S cone pedicle. Note a Landolt's club (black arrow) arises from the dendritic tree and terminates in the layer of cone axons. Dendritic contacts of the FMB cell contacting S cone 5 and neighboring LM cones (indicated by the red arrowheads). Telodendria arising from LM cones 24 and 13 are also noted (black arrows). (*C*) Another view of the morphology of the Landolt's club, which appears as a large accessory dendritic process (*SI Appendix*, Fig. S8). (*D*) Zoomed view of the axon terminals of the S cone 5 contacting FMB cell (FMB 13; teal) and the LM cone contacting FMB cell (FMB 27; yellow) that are enveloped by the dendritic arborization of an OFF-midget ganglion cell (arrow indicates FMB axons; open arrowhead indicates axon terminal arborization; S-FMB 13 and FMB 27 provided 68% and 32% of total bipolar synaptic input, respectively).

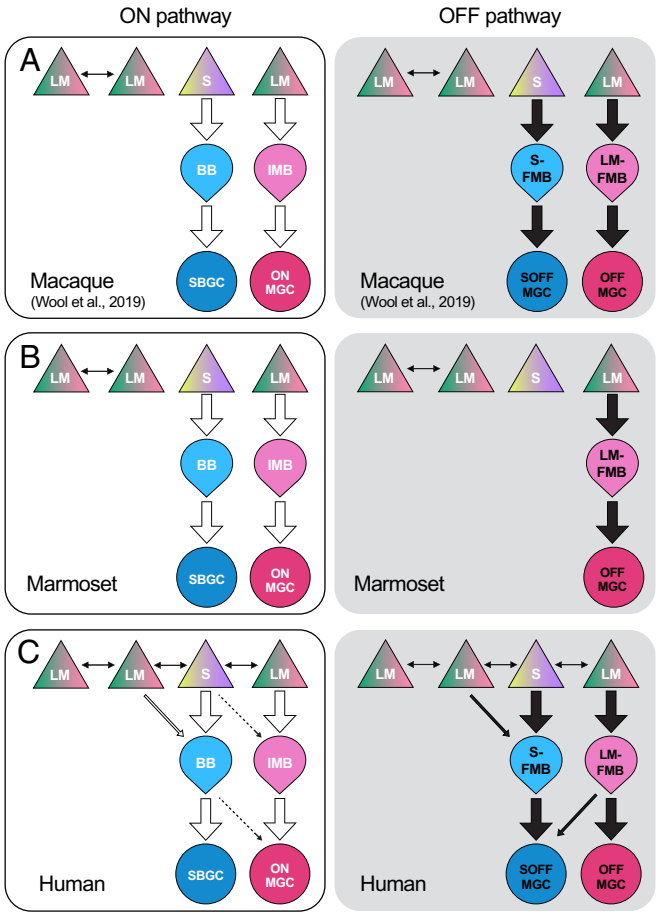

Fig. 7. S-cone wiring in macaque, marmoset, and human retina. (*A*) Canonical, or expected, S cone to bipolar to ganglion cell excitatory connections to the receptive field center derived from previous studies of macaque retina show, 1) Lack or reduction of S cone gap junctions with neighboring LM cones (double-headed arrows indicate cone–cone telodendritic contacts), 2) Selective S cone input to blue cone bipolar cells (S-ON pathway; BB, thick arrow) and selective BB input to small bistratified ganglion cells (SBGC, thick arrow) and, 3) Selective S cone input to a flat midget bipolar cell (S-OFF pathway; S-FMB) and a private-line connection from S-FMB to an S-OFF midget ganglion cell. ON and OFF private-line LM cone midget circuits are also shown (IMB to ONMGC; LM-FMB to OFFMGC). (*B*) Marmoset retina (middle row) shows the canonical pattern with the exception that the S-OFF midget pathway (S-FMB to OFFMGC) is absent. (*C*) S cone circuitry is atypical in human retina. 1) Telodendritic contacts are extensive between S and LM cones (double-headed arrows). 2) The BB (S-ON pathway) draws additional input from neighboring LM cones (thin arrow) and can make synaptic output to ONMGCs (dotted arrow). 3) The S-FMB (S-OFF pathway) draws additional input from neighboring LM cones (thin black arrow) and the LM-FMB can provide additional input to the SOFF-MGC (thin black arrow). Implications for human color vision are considered in the *Discussion*.

the external limiting membrane. The Landolt's club is absent in mammalian retina with the exception of a single Prototherian [egg-laying mammal (81); Echidna; *Tachyglossus aculeatus*]; one early study also suggested their rare presence in both human and chimpanzee retina (82). Here, we find that Landolt's club is a consistent feature of FMB cells in human outer retina (Fig. 6 and *SI Appendix*, Fig. S8). The function of the Landolt's club is unknown, but its presence may reflect the developmental history of bipolar cells and their evolutionary origin from photoreceptors (83). We never observed a Landolt's club on any bipolar cells in either macaque or marmoset retina, so it represents yet another difference in neuronal morphology across these three primate families. The Landolt's club structures do not appear to make synaptic connections and in the context of the present study, we did not consider them further.

Other Noncanonical Features of the Human S Cone Pathway. Our focus so far has been on the ON and OFF circuits associated with the S cone and the distinctive nature of human S cone connectivity. We necessarily explored only a very small space in the retinal connectome. However, other clear examples of noncanonical circuitry were observed and remain to be studied in detail. Most striking was the observation that the human BB axon terminal could synapse on the dendrites of ON-midget ganglion cells deep in the IPL (percent synaptic input: mean ± SD = 8.05 ± 7.53, n = 4). In one example, this connection was extensive, with the BB axon supplying 21% of its ribbon synaptic output (12 of 56 total ribbon synapses) to an ON-midget ganglion cell which also received 19% of its excitatory synaptic input (12 of 65 total synaptic inputs) from this BB cell (*SI Appendix*, Fig. S9 and Fig. 7*C*). By contrast, complete reconstruction of the BB axon terminal in macaque fovea determined that all BB cell synaptic outputs are directed to the SBGC (33). This result is consistent with the conclusion from many physiological studies that in macaques and marmosets, the LM cone midget circuit generates a pure L vs. M cone opponent signal with no S cone contribution (15, 36, 84, 85). A similar interaction of the LM cone ON midget circuit with the S cone was also observed in the outer retina. We found that when LM cones neighbored S cones, LM cone IMB cells could violate private line connectivity and make invaginating contacts with both LM and S cones (percent synaptic input: from neighboring S cone, mean ± SD = 6.55 ± 3.94, from LM cone, mean ± SD = 93.45 ± 3.94; n = 5). Future studies focused on the complete connectome of both the human S cone and BB cell are needed to further assess these observations.

Discussion

Comparative connectomics reveals the anatomical basis for an S-OFF channel in human vision while also demonstrating the absence of this pathway in marmosets. Moreover, the synaptic wiring linked to human S cones showed features not expected based on the nonhuman primate model. We consider these synaptic patterns and the implications for human color vision below. Our assumption that anatomical ribbon synapses from cones to bipolar cells to ganglion cells represent functional excitatory synapses is well supported by extensive studies of ribbon structure and function (86, 87).

S to LM Cone Cross talk in Human Retina. The large, electron-dense telodendritic cone–cone contacts that we observe (Fig. 2 *A* and *B* and *SI Appendix*, Fig. S2 *E–I*) correspond to adherent junctions that each harbor a number of smaller gap junctions (34, 68). The fact that S cones in macaque and marmoset retina appear to lack telodendritic contacts is compatible with previous findings for the blue–green cone networks in ground squirrel retina (88). Paired cone recordings in this species show a clear conductance between green–green cone pairs which is absent for blue–green cone pairs (88). Gap junctional coupling between cones, by averaging uncorrelated noise, is considered an adaptation for improving the signal-to-noise ratio across the cone mosaic (89, 90). The lack of coupling from S to LM cones observed in macaques and marmosets (and other, nonprimate mammals) is consistent with specialization of the mammalian S cone pathway for color processing, likely reflecting a need to keep the S cone signal separate from the LM cone signal until it can be compared at a subsequent chromatic processing stage. Under this interpretation, lack of S to LM cone coupling in macaques and marmosets is consistent with high purity of excitatory S cone signals along the

S vs. LM cone opponent pathway (91, 92). What, then, could explain the presence of S to LM cone coupling we observe in human retina?

We hypothesize that the human S–LM cone–cone coupling could contribute to the early expression of noncardinal cone opponency (e.g., ref. 93). There is already evidence from macaque retina that S cones themselves show LM cone surrounds (via horizontal cell negative feedback) (94) and thus exhibit S vs. LM center-surround cone opponency. If in the human retina, S and LM cone signals are also mixed by even a modest degree of coupling, the S cone would show an elevated response to longer wavelengths (95). Given an LM signal on both sides of the opponent equation, any imbalance in the L vs. M weighting could give rise to S+L vs. M or S+M vs. L receptive fields (31, 85). Thus, initiation of complex and noncardinal opponent signals may begin in the S cone itself in human retina.

The S-OFF Midget Circuit: Present in Humans and Macaques but Absent in Marmosets. Questions to the provenance and nature of S-OFF signals in primate vision are longstanding and remain incompletely resolved (25, 72). The very existence of S-OFF receptive fields was questioned in early single-cell recording studies (96, 97), which seemed to parallel the absence of a clear S-OFF component in both the nonhuman primate (98) and human ERG (99). Although S-OFF cells are now recognized as a consistent functional component of subcortical vision in macaques (100, 101) and marmosets (92, 102), the contributions of S-OFF chromatic signals to human vision remain uncertain (103). Here, we show by connectomic reconstruction from a human fovea that each S cone is presynaptic to an FMB cell identifying a likely first step in the transmission of S-OFF signals to the human central visual pathway. However, the same reconstruction method applied to marmoset retina revealed the clear absence of associated S-FMB cells. Our marmoset retina was acquired from a male obligatory dichromat (expressing a single L or M photopigment in addition to an S photopigment; (see for review, 104), and we cannot rule out the possibility that trichromatic marmoset phenotypes could show a different pattern of S cone connectivity. However, our previous light microscopic immunostaining studies (39, 61) failed to identify S-OFF-associated FMBs at multiple retinal locations in both dichromatic male and trichromatic female marmosets. These results suggest that the clear absence of an S-FMB in marmosets in our data is not related to photopigment polymorphism or retinal eccentricity.

The lack of a marmoset S-OFF midget circuit can be considered in the broader context of the layout and significance of ON and OFF pathways in vertebrate retina. The ON vs. OFF dichotomy is both universal across vertebrate classes (105) and ancient in the evolution of the vertebrates (106). For several of the parallel visual pathways in the most studied mammals, the properties of ON and OFF components show effective mirror symmetry. The most striking examples in marmoset, macaque, and human retina are the ON and OFF midget and ON and OFF parasol ganglion cells. By contrast, ON-OFF symmetry in S cone circuits appears variable. Neither the mouse nor the ground squirrel shows an S cone-selective OFF bipolar cell, in common with what we find here in the marmoset retina. By contrast, rabbit retina does possess an S-OFF bipolar pathway (107), indicating that the marmoset does not simply reflect a shared-derived mammalian circuit motif. Moreover, in both rabbits and ground squirrels, amacrine pathways invert the sign of the S-ON bipolar (107, 108) to create S-OFF cone opponent ganglion cells (109). The answer then to why the S-OFF midget circuit is lacking in marmoset may ultimately be explained more by rapid evolutionary change related to niche-specific differences in visual behavior than by phylogenetic relationships among the mammals. For example, humans are terrestrial, whereas marmosets are strictly arboreal, and macaque species have intermediate lifestyles. The impact of arboreal light environments has been studied in the context of trichromacy in primates as an adaptation for detection of ripe fruit on a dappled background (110, 111). Some mammalian species occupying diverse environments may even lack or show greatly reduced expression of S cone opsin (112, 113), but the impact of environment and lifestyle on the circuitry downstream from the cones themselves remains to be explored. For these and other reasons, such observations may be required to allow sharp predictions linking photoreceptor complement and retinal circuitry to behavior (114).

Noncanonical Wiring Suggests Distinctive Chromatic Tuning in the Human Foveal S Cone Pathways. In macaque retina, a single S cone provides the exclusive excitatory receptor input to both S-ON (BB) and S-OFF (S-FMB) bipolar cells (25) (*SI Appendix*, Fig. S10). This selective S cone input would transmit a pure S cone-driven excitatory receptive field center to downstream S-ON and S-OFF ganglion cells, which are considered the anatomical and physiological substrates for the "blue–yellow" axis in early-stage color processing (45, 115). By contrast, in the human retina, both BB and FMB cells draw excitatory input from LM as well as S cones (Figs. 2 and 6), violating expectations derived primarily from the anatomy and physiology of macaque monkeys (36) (Fig. 7). What do these differences mean for human color vision? The answer may lie in a recent study of midget ganglion cells in the peripheral retina of macaque monkeys that receive S-OFF input (31). In the retinal periphery, midget bipolar cells continue to derive input largely from single cones (116, 117), but the enlarged dendritic trees of midget ganglion cells draw converging input from many midget bipolar cells (61, 85, 118, 119). S-OFF midget ganglion cells in the retinal periphery showed complex chromatic responses combining S cone input with L vs. M opponency (31, see also ref. 120) (e.g., LON vs. M+S OFF or MON vs. L+SOFF). Thus, an imbalance of L and M cone OFF input to the receptive field center vs. surround produces an L vs. M opponent receptive field (84, 85). The sparse S-FMB cell provides an additional S cone input to the receptive field center to shift chromatic tuning away from the canonical L vs. M cardinal axis. In the present study, the convergence of S, L, and M cone inputs in the human retina is distinct in that it occurs at the first synapse between cones and bipolar cells, and in the foveal retina where chromatic circuits are the most well developed (31, 84, 85). In addition, in the human fovea, S-OFF midget ganglion cells begin to sum input from both S and LM cone-connected midget bipolar cells (see Fig. 6 for an example), similar to what has been observed only in the retinal periphery in the macaque retina (30, 31, 35). Our results predict that the addition of LM signals to both S-ON and S-OFF receptive field center (given the opponent LM surround) would produce complex, noncardinal cone opponency similar to that observed in macaque peripheral retina. Such deviations from the cardinal S vs. L+M and L vs. M chromatic axes have been described repeatedly in psychophysical studies of human color vision (23, 93, 121–123) and are customarily attributed to higher-order (i.e., cortical) mechanisms that recombine signals from the cardinal axes emerging from retinal circuitry (17, 19, 124). Evidence for such recombination in macaque monkeys has been provided for both primary visual cortex (24) and cortical area V4 (125, 126). Our results suggest that for

humans, variation in synaptic connectivity could impact spectral tuning of chromatic pathways (127) even at the first synapse in the visual system.

Materials and Methods

The methods for human, macaque, and marmoset tissue acquisition and serial block-face scanning electron microscopy sample preparation, image acquisition, circuit reconstruction, and statistical analyses are described in *SI Appendix, Materials and Methods*.

Data, Materials, and Software Availability. All study data are included in the article and/or *SI Appendix*.

ACKNOWLEDGMENTS. This work was supported by NIH grant EY-028282 to D.M.D. and by NIH Grant RR-00166 to the Tissue Distribution Program of the Washington National Primate Research Center (WaNPRC), grant P51 OD010425 from the NIH Office of Research Infrastructure Program to the WaNPRC, and EY01730 to the Vision Research Core at the University of Washington. We thank Sharm Knecht for tissue preparation for electron microscopy and managing connectomics data acquisition, Rob Smith for advice, and Marcello Rosa for making marmoset tissue available.

Author affiliations: [a]Department of Biological Structure, University of Washington, Seattle, WA 98195; [b]Department of Ophthalmology, Medical University of Vienna, Vienna 1090, Austria; [c]Save Sight Institute and Department of Ophthalmology, Faculty of Medicine and Health, The University of Sydney, Sydney, NSW 2000, Australia; and [d]Washington National Primate Research Center, University of Washington, Seattle, WA 98195

1. L. F. Abbott *et al.*, The mind of a mouse. *Cell* **182**, 1372–1376 (2020).
2. E. A. Buffalo, J. A. Movshon, R. H. Wurtz, From basic brain research to treating human brain disorders. *Proc. Natl. Acad. Sci. U.S.A.* **116**, 26167–26172 (2019).
3. N. Jourjine, H. E. Hoekstra, Expanding evolutionary neuroscience: Insights from comparing variation in behavior. *Neuron* **109**, 1084–1099 (2021).
4. R. J. V. Roberts, S. Pop, L. L. Prieto-Godino, Evolution of central neural circuits: State of the art and perspectives. *Nat. Rev. Neurosci.* **23**, 725–743 (2022).
5. E. Barsotti, A. Correia, A. Cardona, Neural architectures in the light of comparative connectomics. *Curr. Opin. Neurobiol.* **71**, 139–149 (2021).
6. M. E. Hale, Mapping circuits beyond the models: Integrating connectomics and comparative neuroscience. *Neuron* **83**, 1256–1258 (2014).
7. D. S. Galili, G. S. Jefferis, M. Costa, Connectomics and the neural basis of behaviour. *Curr. Opin. Insect. Sci.* **54**, 100968 (2022).
8. I. A. Meinertzhagen, "Perspective: A new era of comparative connectomics" in *Decoding Neural Circuit Structure and Function*, C. Arzu, M. F. Wernet, Eds. (Springer International AG, New York, 2017).
9. M. I. Sereno, R. B. Tootell, From monkeys to humans: What do we now know about brain homologies? *Curr. Opin. Neurobiol.* **15**, 135–144 (2005).
10. T. M. Preuss, "Specializations of the human visual system: The monkey model meets human reality" in *The Primate Visual System*, J. H. Kass, C. E. Collins, Eds. (CRC Press, Boca Raton, Fl, 2004), pp. 231–259.
11. N. Takahata, Y. Satta, Evolution of the primate lineage leading to modern humans: Phylogenetic and demographic inferences from DNA sequences. *Proc. Natl. Acad. Sci. U.S.A.* **94**, 4811–4815 (1997).
12. H. Hofer, J. Carroll, J. Neitz, M. Neitz, D. Williams, Organization of the human trichromatic cone mosaic. *J. Neurosci.* **25**, 9669–9679 (2005).
13. D. A. Baylor, B. J. Nunn, J. L. Schnapf, Spectral sensitivity of cones of the monkey *Macaca fascicularis*. *J. Physiol. (Lond.)* **390**, 145–160 (1987).
14. B. P. Schmidt, A. E. Boehm, W. S. Tuten, A. Roorda, Spatial summation of individual cones in human color vision. *PLoS One* **14**, e0211397 (2019).
15. A. M. Derrington, J. Krauskopf, P. Lennie, Chromatic mechanisms in lateral geniculate nucleus of macaque. *J. Physiol. (Lond.)* **357**, 241–265 (1984).
16. J. D. Mollon, G. Jordan, "On the nature of unique hues" in *John Dalton's Colour Vision Legacy*, C. Dickinson, I. Murray, D. Carden, Eds. (Taylor & Francis, London, 1997), pp. 381–392.
17. A. Stockman, D. H. Brainard, "Color vision mechanisms" in *OSA Handbook of Optics*, M. Bass, Ed. (McGraw-Hill, ed. 3, New York, 2010), pp. 11.11–11.104.
18. S. K. Shevell, P. R. Martin, Color opponency: Tutorial. *J. Opt. Soc. Am. A Opt. Image Sci. Vis.* **34**, 1099–1108 (2017).
19. M. A. Webster, E. Miyahara, G. Malkoc, V. E. Raker, Variations in normal color vision. II. Unique hues. *J. Opt. Soc. Am. A Opt. Image Sci. Vis.* **17**, 1545–1555 (2000).
20. S. M. Wuerger, P. Atkinson, S. Cropper, The cone inputs to the unique-hue mechanisms. *Vision Res.* **45**, 3210–3223 (2005).
21. M. A. Webster, The Verriest lecture: Adventures in blue and yellow. *J. Opt. Soc. Am. A Opt. Image Sci. Vis.* **37**, V1–V14 (2020).
22. R. L. DeValois, N. P. Cottaris, S. D. Elfar, L. E. Mahon, J. A. Wilson, Some transformations of color information from lateral geniculate nucleus to striate cortex. *Proc. Natl. Acad. Sci. U.S.A.* **97**, 4997–5002 (2000).
23. R. L. DeValois, K. K. DeValois, L. E. Mahon, Contribution of S opponent cells to color appearance. *Proc. Natl. Acad. Sci. U.S.A.* **97**, 512–517 (2000).
24. P. Li, A. K. Garg, L. A. Zhang, M. S. Rashid, E. M. Callaway, Cone opponent functional domains in primary visual cortex combine signals for color appearance mechanisms. *Nat. Commun.* **13**, 6344 (2022).
25. D. M. Dacey, J. D. Crook, O. S. Packer, Distinct synaptic mechanisms create parallel S-ON and S-OFF color opponent pathways in the primate retina. *Vis. Neurosci.* **31**, 139–151 (2014).
26. S. Herr, K. Klug, P. Sterling, S. Schein, Inner S-cone bipolar cells provide all of the central elements for S cones in macaque retina. *J. Comp. Neurol.* **457**, 185–201 (2003).
27. D. M. Dacey, Morphology of a small-field bistratified ganglion cell type in the macaque and human retina. *Vis. Neurosci.* **10**, 1081–1098 (1993).
28. Y. Tsukamoto, N. Omi, ON bipolar cells in macaque retina: Type-specific synaptic connectivity with special reference to OFF counterparts. *Front. Neuroanat.* **10**, 104 (2016).
29. U. Grünert, P. R. Martin, Cell types and cell circuits in human and non-human primate retina. *Prog. Retin. Eye Res.*, 10.1016/j.preteyeres.2020.100844 (2020).
30. K. Klug, S. Herr, I. T. Ngo, P. Sterling, S. Schein, Macaque retina contains an S-cone OFF midget pathway. *J. Neurosci.* **23**, 9881–9887 (2003).
31. L. E. Wool, O. S. Packer, Q. Zaidi, D. M. Dacey, Connectomic identification and three-dimensional color tuning of S-OFF midget ganglion cells in the primate retina. *J. Neurosci.* **39**, 7893–7909 (2019).
32. D. M. Dacey, B. B. Lee, The blue-ON opponent pathway in primate retina originates from a distinct bistratified ganglion cell type. *Nature* **367**, 731–735 (1994).
33. D. J. Calkins, Y. Tsukamoto, P. Sterling, Microcircuitry and mosaic of a blue-yellow ganglion cell in the primate retina. *J. Neurosci.* **18**, 3373–3385 (1998).
34. J. J. O'Brien, X. Chen, P. R. Macleish, J. O'Brien, S. C. Massey, Photoreceptor coupling mediated by connexin36 in the primate retina. *J. Neurosci.* **32**, 4675–4687 (2012).
35. S. S. Patterson *et al.*, An S-cone circuit for edge detection in the primate retina. *Sci. Rep.* **9**, 11913 (2019).
36. S. Solomon, P. Lennie, The machinery of colour vision. *Nat. Rev. Neurosci.* **8**, 276–286 (2007).
37. D. J. Calkins, Seeing with S cones. *Prog. Retin. Eye Res.* **20**, 255–287 (2001).
38. H. Kolb, P. Goede, S. Roberts, R. McDermott, P. Gouras, Uniqueness of the S-cone pedicle in the human retina and consequences for color processing. *J. Comp. Neurol.* **386**, 443–460 (1997).
39. S. C. Lee, I. Telkes, U. Grünert, S-cones do not contribute to the OFF-midget pathway in the retina of the marmoset, Callithrix jacchus. *Eur. J. Neurosci.* **22**, 437–447 (2005).
40. K. K. Ghosh, P. R. Martin, U. Grünert, Morphological analysis of the blue cone pathway in the retina of a new world monkey, the marmoset *Callithrix jacchus*. *J. Comp. Neurol.* **379**, 211–225 (1997).
41. K. K. Ghosh, U. Grünert, Synaptic input to small bistratified (blue-ON) ganglion cells in the retina of a new world monkey, the marmoset Callithrix jacchus. *J. Comp. Neurol.* **413**, 417–428 (1999).
42. A. Onishi *et al.*, Vision–Dichromatism in macaque monkeys. *Nature* **402**, 139–140 (1999).
43. G. H. Jacobs, G. A. Williams, The prevalence of defective color vision in Old World monkeys and apes. *Proc. Int. Colour Vision Soc.* **26**, S123–S127 (2001).
44. G. H. Jacobs, Primate color vision: A comparative perspective. *Vis. Neurosci.* **25**, 619–633 (2008).
45. W. B. Thoreson, D. M. Dacey, Diverse cell types, circuits, and mechanisms for color vision in the vertebrate retina. *Physiol. Rev.* **99**, 1527–1573 (2019).
46. W. Yan *et al.*, Cell atlas of the human fovea and peripheral retina. *Sci. Rep.* **10**, 9802 (2020).
47. Y. R. Peng *et al.*, Molecular classification and comparative taxonomics of foveal and peripheral cells in primate retina. *Cell* **176**, 1222–1237.e22 (2019).
48. H. Ding, R. G. Smith, A. Poleg-Polsky, J. S. Diamond, K. L. Briggman, Species-specific wiring for direction selectivity in the mammalian retina. *Nature* **535**, 105–110 (2016).
49. D. J. Calkins, S. J. Schein, Y. Tsukamoto, P. Sterling, M and L cones in macaque fovea connect to midget ganglion cells by different numbers of excitatory synapses. *Nature* **371**, 70–72 (1994).
50. C. A. Curcio *et al.*, Distribution and morphology of human cone photoreceptors stained with anti-blue opsin. *J. Comp. Neurol.* **312**, 610–624 (1991).
51. K. C. Wikler, P. Rakic, Distribution of photoreceptor subtypes in the retina of diurnal and nocturnal primates. *J. Neurosci.* **10**, 3390–3401 (1990).
52. P. R. Martin, U. Grünert, Analysis of the short wavelength-sensitive ("blue") cone mosaic in the primate retina: Comparison of New World and Old World monkeys. *J. Comp. Neurol.* **406**, 1–14 (1999).
53. P. R. Martin, U. Grünert, T. L. Chan, K. Bumsted, Spatial order in short-wavelength-sensitive cone photoreceptors: A comparative study of the primate retina. *J. Opt. Soc. Am. A Opt. Image Sci. Vis.* **17**, 557–567 (2000).
54. S. Lee, U. Grünert, Connections of diffuse bipolar cells in primate retina are biased against S-cones. *J. Comp. Neurol.* **502**, 126–140 (2007).
55. P. Ahnelt, C. Keri, H. Kolb, Identification of pedicles of putative blue-sensitive cones in the human retina. *J. Comp. Neurol.* **293**, 39–53 (1990).
56. A. P. Mariani, Bipolar cells in monkey retina selective for the cones likely to be blue-sensitive. *Nature* **308**, 184–186 (1984).
57. N. Kouyama, D. W. Marshak, Bipolar cells specific for blue cones in the macaque retina. *J. Neurosci.* **12**, 1233–1252 (1992).
58. B. B. Boycott, H. Wässle, Morphological classification of bipolar cells of the primate retina. *Eur. J. Neurosci.* **3**, 1069–1088 (1991).
59. K. A. Percival, P. R. Jusuf, P. R. Martin, U. Grünert, Synaptic inputs onto small bistratified (blue-ON/yellow-OFF) ganglion cells in marmoset retina. *J. Comp. Neurol.* **517**, 655–669 (2009).
60. P. Jusuf, P. Martin, U. Grünert, Synaptic connectivity in the midget-parvocellular pathway of primate central retina. *J. Comp. Neurol.* **494**, 260–274 (2006).
61. I. Telkes, S. C. Lee, P. R. Jusuf, U. Grünert, The midget-parvocellular pathway of marmoset retina: A quantitative light microscopic study. *J. Comp. Neurol.* **510**, 539–549 (2008).
62. D. M. Dacey, The mosaic of midget ganglion cells in the human retina. *J. Neurosci.* **13**, 5334–5355 (1993).
63. H. Kolb, D. Marshak, The midget pathways of the primate retina. *Documenta ophthalmologica. Adv. Ophthalmol.* **106**, 67–81 (2003).
64. H. Kolb, L. Dekorver, Midget ganglion cells of the parafovea of the human retina: A study by electron microscopy and serial section reconstructions. *J Comp. Neurol.* **303**, 617–636 (1991).
65. H. Kolb, K. A. Linberg, S. K. Fisher, Neurons of the human retina: A Golgi study. *J. Comp. Neurol.* **318**, 147–187 (1992).
66. P. K. Ahnelt, H. Kolb, R. Pflug, Identification of a subtype of cone photoreceptor, likely to be blue sensitive, in the human retina. *J. Comp. Neurol.* **255**, 18–34 (1987).
67. C. Puller, S. Haverkamp, U. Grünert, OFF midget bipolar cells in the retina of the marmoset, Callithrix jacchus, express AMPA receptors. *J. Comp. Neurol.* **502**, 442–454 (2007).

68. Y. Tsukamoto, P. Masarachia, S. J. Schein, P. Sterling, Gap junctions between the pedicles of macaque foveal cones. *Vision Res.* **32**, 1809–1815 (1992).
69. T. L. Chan, P. R. Martin, N. Clunas, U. Grünert, Bipolar cell diversity in the primate retina: Morphologic and immunocytochemical analysis of a New World monkey, the marmoset Callithrix jacchus. *J. Comp. Neurol.* **437**, 219–239 (2001).
70. X. G. Luo, K. K. Ghosh, P. R. Martin, U. Grünert, Analysis of two types of cone bipolar cells in the retina of a New World monkey, the marmoset, *Callithrix jacchus*. *Vis. Neurosci.* **16**, 707–719 (1999).
71. R. A. Masri, K. A. Percival, A. Koizumi, P. R. Martin, U. Grünert, Survey of retinal ganglion cell morphology in marmoset. *J. Comp. Neurol.* **527**, 236–258 (2019).
72. K. J. Miyagishima, U. Grünert, W. Li, Processing of S-cone signals in the inner plexiform layer of the mammalian retina. *Vis. Neurosci.* **31**, 153–163 (2014).
73. O. Kantor *et al.*, Characterization of connexin36 gap junctions in the human outer retina. *Brain Struct. Funct.* **221**, 2963–2984 (2016).
74. S. Haverkamp *et al.*, The primordial, blue-cone color system of the mouse retina. *J. Neurosci.* **25**, 5438–5445 (2005).
75. W. Li, S. DeVries, Bipolar cell pathways for color and luminance vision in a dichromatic mammalian retina. *Nat. Neurosci.* **9**, 669–675 (2006).
76. M. A. MacNeil, P. A. Gaul, Biocytin wide-field bipolar cells in rabbit retina selectively contact blue cones. *J. Comp. Neurol.* **506**, 6–15 (2008).
77. Y. Tsukamoto, N. Omi, OFF bipolar cells in macaque retina: Type-specific connectivity in the outer and inner synaptic layers. *Front. Neuroanat.* **9**, 122 (2015).
78. S. M. Wu, F. Gao, B. R. Maple, Functional architecture of synapses in the inner retina: Segregation of visual signals by stratification of bipolar cell axon terminals. *J. Neurosci.* **20**, 4462–4470 (2000).
79. A. Günther *et al.*, Double cones and the diverse connectivity of photoreceptors and bipolar cells in an avian retina. *J. Neurosci.* **41**, 5015–5028 (2021).
80. A. Quesada, V. Garcia-Lomas, J. M. Genis-Galvez, The midget bipolar cells in the chick retina. *Curr. Eye Res.* **5**, 85–92 (1986).
81. H. M. Young, D. I. Vaney, The retinae of Prototherian mammals possess neuronal types that are characteristic of non-mammalian retinae. *Vis. Neurosci.* **5**, 61–66 (1990).
82. S. L. Polyak, *The Retina* (University of Chicago Press, Chicago, 1941).
83. T. D. Lamb, Evolution of phototransduction, vertebrate photoreceptors and retina. *Prog. Retin. Eye Res.* **36**, 52–119 (2013).
84. P. R. Martin, E. M. Blessing, P. Buzas, B. A. Szmajda, J. D. Forte, Transmission of colour and acuity signals by parvocellular cells in marmoset monkeys. *J. Physiol.* **589**, 2795–2812 (2011).
85. L. E. Wool *et al.*, Nonselective wiring accounts for red-green opponency in midget ganglion cells of the primate retina. *J. Neurosci.* **38**, 1520–1540 (2018).
86. W. B. Thoreson, Transmission at rod and cone ribbon synapses in the retina. *Pflugers Arch.* **473**, 1469–1491 (2021).
87. T. Moser, C. P. Grabner, F. Schmitz, Sensory processing at ribbon synapses in the retina and the cochlea. *Physiol. Rev.* **100**, 103–144 (2020).
88. W. Li, S. H. DeVries, Separate blue and green cone networks in the mammalian retina. *Nat. Neurosci.* **7**, 751–756 (2004).
89. S. H. DeVries, X. Qi, R. Smith, W. Makous, P. Sterling, Electrical coupling between mammalian cones. *Curr. Biol. CB* **12**, 1900–1907 (2002).
90. E. P. Hornstein, J. Verweij, J. L. Schnapf, Electrical coupling between red and green cones in primate retina. *Nat. Neurosci.* **7**, 745–750 (2004).
91. J. D. Crook *et al.*, Parallel ON and OFF cone bipolar inputs establish spatially coextensive receptive field structure of blue-yellow ganglion cells in primate retina. *J. Neurosci.* **29**, 8372–8387 (2009).
92. C. D. Eiber, A. N. J. Pietersen, N. Zeater, S. G. Solomon, P. R. Martin, Chromatic summation and receptive field properties of blue-on and blue-off cells in marmoset lateral geniculate nucleus. *Vision Res.* **151**, 41–52 (2018).
93. M. V. Danilova, J. D. Mollon, Cardinal axes are not independent in color discrimination. *J. Opt. Soc. Am. A Opt. Image Sci. Vis.* **29**, A157–A164 (2012).
94. O. S. Packer, J. Verweij, P. H. Li, J. L. Schnapf, D. M. Dacey, Blue-yellow opponency in primate S cone photoreceptors. *J. Neurosci.* **30**, 568–572 (2010).
95. A. Hsu, R. G. Smith, G. Buchsbaum, P. Sterling, Cost of cone coupling to trichromacy in primate fovea. *J. Opt. Soc. Am. A Opt. Image Sci. Vis.* **17**, 635–640 (2000).
96. F. M. de Monasterio, Asymmetry of On-and OFF-pathways of blue-sensitive cones of the retina of macaques. *Brain Res.* **166**, 39–48 (1979).
97. E. Zrenner, P. Gouras, Characteristics of the blue sensitive cone mechanism in primate retinal ganglion cells. *Vision Res.* **21**, 1605–1609 (1981).
98. H. U. Evers, P. Gouras, Three cone mechanisms in the primate electroretinogram: Two with, one without off-center bipolar responses. *Vis. Res.* **26**, 245–254 (1986).
99. P. Gouras, C. J. MacKay, S. Yamamoto, The human S-cone electroretinogram and its variation among subjects with and without L and M-cone function. *Invest. Ophthalmol. Vis. Sci* **34**, 2437–2442 (1993).
100. A. Valberg, B. B. Lee, D. A. Tigwell, Neurones with strong inhibitory s-cone inputs in the macaque lateral geniculate nucleus. *Vision Res.* **26**, 1061–1064 (1986).
101. C. Tailby, S. G. Solomon, P. Lennie, Functional asymmetries in visual pathways carrying S-cone signals in macaque. *J. Neurosci.* **28**, 4078–4087 (2008).
102. P. R. Martin, B. B. Lee, Distribution and specificity of S-cone ("blue cone") signals in subcortical visual pathways. *Vis. Neurosci.* **31**, 177–187 (2014).
103. H. E. Smithson, S-cone psychophysics. *Vis. Neurosci.* **31**, 211–225 (2014).
104. G. H. Jacobs, New World monkeys and color. *Int. J. Primatol.* **28**, 729–759 (2007).
105. R. Nelson, H. Kolb, "ON and OFF pathways in the vertebrate visual system" in *The Visual Neurosciences*, L. M. Chalupa, J. S. Werner, Eds. (MIT press, Cambridge, AA, 2004).
106. E. M. Ellis, R. Frederiksen, A. Morshedian, G. L. Fain, A. P. Sampath, Separate ON and OFF pathways in vertebrate vision first arose during the Cambrian. *Curr. Biol.* **30**, R633–R634 (2020).
107. S. L. Mills, L. M. Tian, H. Hoshi, C. M. Whitaker, S. C. Massey, Three distinct blue-green color pathways in a mammalian retina. *J. Neurosci.* **34**, 1760–1768 (2014).
108. S. Chen, W. Li, A color-coding amacrine cell may provide a blue-off signal in a mammalian retina. *Nat. Neurosci.* **15**, 954–956 (2012).
109. A. Sher, S. H. DeVries, A non-canonical pathway for mammalian blue-green color vision. *Nat. Neurosci.* **15**, 952–953 (2012).
110. B. C. Regan *et al.*, Fruits, foliage and the evolution of primate colour vision. *Philos. Trans. R Soc. Lond. B Biol. Sci.* **356**, 229–283 (2001).
111. P. Sumner, J. D. Mollon, Chromaticity as a signal of ripeness in fruits taken by primates. *J. Exp. Biol.* **203**, 1987–2000 (2000).
112. D. M. Hunt, L. Peichl, S cones: Evolution, retinal distribution, development, and spectral sensitivity. *Vis. Neurosci.* **31**, 115–138 (2014).
113. G. H. Jacobs, Losses of functional opsin genes, short-wavelength cone photopigments, and color vision–A significant trend in the evolution of mammalian vision. *Vis. Neurosci.* **30**, 39–53 (2013).
114. T. Baden, T. Euler, P. Berens, Understanding the retinal basis of vision across species. *Nat. Rev. Neurosci.* **21**, 5–20 (2020).
115. P. Lennie, J. A. Movshon, Coding of color and form in the geniculostriate visual pathway (invited review). *J. Opt. Soc. Am. A Opt. Image Sci. Vis.* **22**, 2013–2033 (2005).
116. H. Wässle, U. Grünert, P. R. Martin, B. B. Boycott, Immunocytochemical characterization and spatial distribution of midget bipolar cells in the macaque monkey retina. *Vision Res.* **34**, 561–579 (1994).
117. A. H. Milam, D. M. Dacey, A. M. Dizhoor, Recoverin immunoreactivity in mammalian cone bipolar cells. *Vis. Neurosci.* **10**, 1–12 (1993).
118. P. Jusuf, P. Martin, U. Grünert, Random wiring in the midget pathway of primate retina. *J. Neurosci.* **26**, 3908–3917 (2006).
119. Y. J. Kim *et al.*, Origins of direction selectivity in the primate retina. *Nat. Commun.* **13**, 2862 (2022).
120. F. M. de Monasterio, P. Gouras, D. J. Tolhurst, Trichromatic color opponency in ganglion cells of the rhesus monkey retina. *J. Physiol. (Lond.)* **251**, 197–216 (1975).
121. C. F. Stromeyer III, *et al.*, Short-wave cone signal in the red-green detection mechanism. *Vision Res.* **38**, 813–826 (1998).
122. M. V. Danilova, J. D. Mollon, Discrimination of hue angle and discrimination of colorimetric purity assessed with a common metric. *J. Opt. Soc. Am. A Opt. Image Sci. Vis.* **37**, A226–A236 (2020).
123. M. A. Webster, J. D. Mollon, Changes in colour appearance following post-receptoral adaptation. *Nature* **349**, 235–238 (1991).
124. R. L. DeValois, K. K. DeValois, A multi-stage color model. *Vision Res.* **33**, 1053–1065 (1993).
125. K. S. Bohon, K. L. Hermann, T. Hansen, B. R. Conway, Representation of perceptual color space in macaque posterior inferior temporal cortex (the v4 complex). *eNeuro* **3**, ENEURO.0039-16.2016 (2016).
126. B. N. Bushnell, P. J. Harding, Y. Kosai, W. Bair, A. Pasupathy, Equiluminance cells in visual cortical area v4. *J. Neurosci.* **31**, 12398–12412 (2011).
127. M. A. Webster, E. Miyahara, G. Malkoc, V. E. Raker, Variations in normal color vision. I. Cone-opponent axes. *J. Opt. Soc. Am. A Opt. Image Sci. Vis.* **17**, 1535–1544 (2000).